Next Generation Very Large Array Memo No. 95: Evaluation of the Revision D array configuration for stellar imaging

Catherine Petretti [1,2] Kazunori Akiyama [2,3,4] and Lynn D. Matthews [2]

[1] Department of Astrophysics & Planetary Science, Villanova University, 800 Lancaster Ave, Villanova, PA, 19085, USA
[2] Massachusetts Institute of Technology Haystack Observatory, 99 Millstone Road, Westford, MA 01886, USA
[3] National Astronomical Observatory of Japan, 2-21-1 Osawa, Mitaka, Tokyo 181-8588, Japan
[4] Black Hole Initiative, Harvard University, 20 Garden Street, Cambridge, MA 02138, USA

ABSTRACT

A transformative science case for the proposed next-generation Very Large Array (ngVLA) is resolving the surfaces of nearby stars, both spatially and temporally, enabled by the combination of milliarcsecond-scale resolution and unprecedented sensitivity to thermal radio emission. In a previous study, we demonstrated the feasibility of stellar imaging with simulated observations of nearby stars, using both traditional `CLEAN` techniques and newly developed regularized maximum likelihood (RML) imaging methods for image reconstruction. In this memo, we present a continued study of stellar imaging with the ngVLA, evaluating the imaging capability of the Revision D (henceforth Rev D) Main Array configuration compared to the previous Revision C (henceforth Rev C) configuration. We find that the Rev D configuration, with more uniform coverage and better circular symmetry, improves the synthesized beam, resulting in better `CLEAN` reconstructions of simulated images of evolved stars with complex morphology, especially with robust weighting. However, the highly non-Gaussian nature of the synthesized beam still persists with both robust and natural weightings in the Rev D configuration and continues to limit the image fidelity of image reconstructions with non-uniform weighting. The RML methods show stable performance that is resilient to different array configurations with image quality comparable to or better than `CLEAN` methods in the presented simulation, consistent with our previous work. Our simulation results suggest that the Rev D configuration will provide a better deconvolution beam compared with the Rev C configuration, which would enhance the imaging capability for non-uniform weighting, and they continue to demonstrate that RML methods are an attractive choice, even for the improved array configuration.

1. INTRODUCTION

The next-generation Very Large Array (ngVLA) is currently planned to be a heterogeneous array of 244 antennas of 18 m diameter and 19 dishes with 6 m diameter (Selina et al. 2018), with the array design based on designated "key science goals" (Murphy et al. 2018). To meet diverse scientific needs, the planned ngVLA array is designed to have three subarrays: a "Short Baseline Array" with baselines of 11–56 m, a "Main Array" with 214 of the 18 m antennas on baselines ranging from tens of meters to ∼1000 km, and a "Long Baseline Array" with 30 of the 18 m antennas spread across the North American continent for Very Long Baseline Interferometry (VLBI).

The ngVLA Main Array will be able to detect thermal emission at milliarcsecond-scale resolution. Until now, such angular scales have only been accessible with VLBI for compact, non-thermal objects with a high brightness temperature. A groundbreaking scientific application of the Main Array will be its ability to obtain resolved images of the surfaces of nearby stars spanning a range of spectral types and evolutionary phases from dwarfs to supergiants (Carilli et al. 2018; Matthews & Claussen 2018; Harper 2018; Akiyama & Matthews 2019).

The current ngVLA design has a Main Array that is "tri-scaled" (e.g. Carilli 2017, 2018), comprising: (1) a densely sampled, 1 km-diameter core of 94 antennas; (2) a VLA-scale array of 74 antennas with baselines up to ∼30 km; and (3) extended baselines (46 stations) out to ∼1000 km. Although the Main Array is suited to meeting the ngVLA's combined requirements for angular resolution, point source sensitivity, and surface brightness sensitivity, its antenna distribution results in a highly non-Gaussian synthesized beam. The beam shape comprises a narrow core and a two-tiered "skirt," or long tail of side lobes (Carilli 2017, 2018). This poses a challenge

for imaging ngVLA data with traditional CLEAN deconvolution methods, in which a model of the ideal "CLEAN beam" is determined by fitting a Gaussian to the dirty beam point spread function (e.g., Högbom 1974). A consequence is that it is difficult to achieve maximum angular resolution in an ngVLA CLEAN image without sacrificing sensitivity (Carilli 2017, 2018; Rosero 2019). This issue cannot be overcome through the use of robust weighting (Briggs et al. 1999) during the deconvolution (Carilli 2017), and it therefore currently presents a potential inherent limitation to the array performance.

1.1. *Our previous study*

In a previous ngVLA study (ngVLA memo No. 66; Akiyama & Matthews 2019), we investigated the application of regularized maximum likelihood (RML) methods (see EHT Collaboration 2019, for an overview), a new class of imaging techniques developed for the Event Horizon Telescope, to simulate ngVLA Main Array observations of stellar radio photospheres as a test case. RML methods take a forward-modeling approach, directly solving for the images without using either the dirty beam or the dirty map. Consequently, this method has the potential to improve the fidelity and effective angular resolution of ngVLA images in three ways: (1) allowing high-fidelity reconstructions, even at modest super resolution 2-3 times finer than that of traditional CLEAN (e.g. Honma et al. 2014; Chael et al. 2016; Akiyama et al. 2017a,b; Kuramochi et al. 2018); (2) the capability to reconstruct images directly from closure quantities, free from antenna-based calibration errors (e.g. Chael et al. 2016, 2018; Akiyama et al. 2017b); and (3) the ability to handle intrinsically multi-dimensional emission, such as time-variable emission structures (e.g. Johnson et al. 2017). The aforementioned advantages of RML methods over CLEAN have now been demonstrated not only for VLBI but also for VLA and ALMA continuum observations (Matthews et al. 2018a; Chael et al. 2018; Yamaguchi et al. 2020).

We found that both Multi-scale CLEAN (henceforth MS-CLEAN; Cornwell 2008) and RML methods can provide high-fidelity images recovering most of the representative structures for different types of stellar photosphere models imaged with the ngVLA. However, RML methods show better performance than MS-CLEAN for various stellar models in terms of goodness-of-fit to the data, residual errors of the images, and recovering representative features in the groundtruth images. Our simulations support the feasibility of transformative stellar imaging science with the ngVLA and simultaneously demonstrate that RML methods are an attractive choice for ngVLA imaging.

1.2. *Revision D array configuration and scope of this memo*

An updated planned configuration of the ngVLA Main Array, Revision D (hereafter Rev D), was recently developed by the ngVLA Imaging and Calibration Working Group as part of Conceptual Design Review (CoDR) preparation (Carilli et al. 2021). The Rev D configuration has many updates from the previous configuration, revision C.01[1] (henceforth Rev C) adopted in our previous memo (Akiyama & Matthews 2019). The major changes in the Main Array relative to the Rev C configuration include: (1) the 46 antennas for extended baselines from ∼30 km to ∼1000 km are more distributed; and (2) the central core array with 94 antennas has been expanded substantially from ∼1 km to ∼4 km.

The updated Rev D design exhibits substantial changes in the antenna positions from the previous revision. In Figure 1, we show the antenna positions of both the Rev C and Rev D configurations. The Rev D design has five "spiral arms" of antennas, providing extended baseline lengths ranging from ∼30 km to ∼1000 km, whose shapes are much clearer than the Rev C design. The antenna positions are more evenly distributed both along each arm and between arms, which may provide substantial improvements in *uv*-coverage (see Section 2.2).

In this memo we continue the work of Akiyama & Matthews (2019) by evaluating the imaging capability of the Rev D configuration for stellar imaging. We performed imaging simulations of several stellar photosphere models using MS-CLEAN and RML methods with both Rev C and Rev D configurations to assess the improvement with the updated array configuration. In CLEAN imaging, we also explore the performance of different *uv*-weightings, whereas our previous work only explored uniform weighting.

2. MODELS AND SIMULATED OBSERVATIONS

2.1. *Models*

We evaluated the imaging performance for both the Rev C and Rev D configurations using a series of four different simulated data sets, adopted in our previous study (Akiyama & Matthews 2019). Here, we briefly describe each model. For more details, please see Akiyama & Matthews (2019).

The first series of models comprises simple geometric disk models based on a uniform disk brightness distribution with surface features superposed. This class of models is motivated by the observed brightness dis-

[1] available in https://ngvla.nrao.edu/page/tools

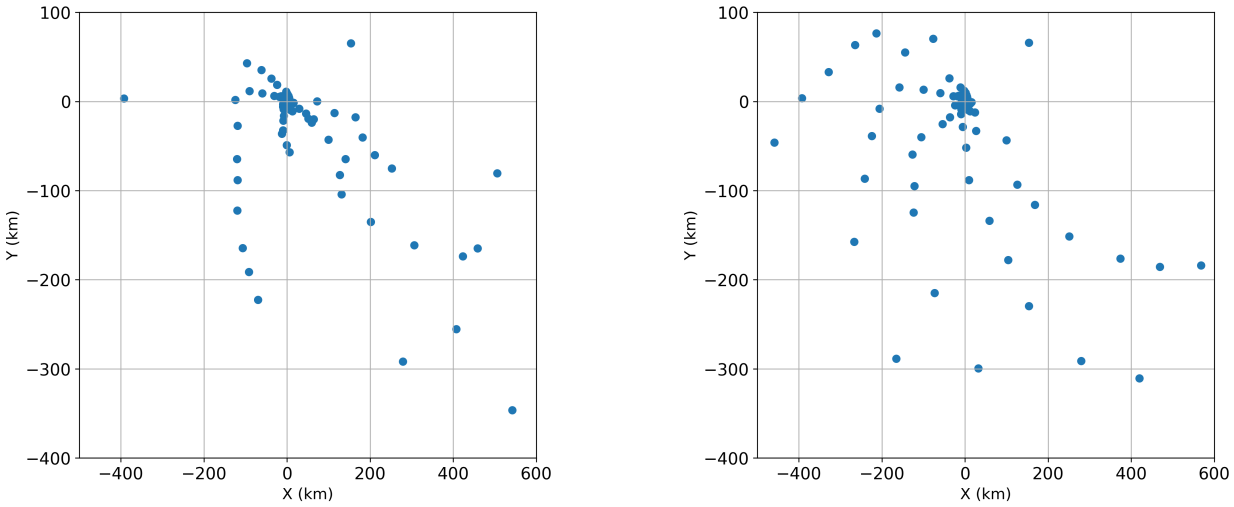

(a) Rev C Configuration

(b) Rev D Configuration

Figure 1. Baseline configurations of (a) Rev C and (b) Rev D Main Arrays for the ngVLA.

tribution of the radio photospheres of nearby asymptotic giant branch (AGB) and red supergiant (RSG) stars, whose radio emission are well represented by a uniform disk (either circular or elliptical) at the angular resolutions of the current VLA and ALMA (∼20–40 mas), which is sufficient only to marginally resolve the radio photospheres of the nearest AGB and RSG stars (e.g., Lim et al. 1998; Reid & Menten 1997, 2007; Menten et al. 2012; Matthews et al. 2015, 2018b; Vlemmings et al. 2017). We adopted two models created in our previous memo, `UniDisk222pc` and `UniDisk1kpc`, with uniform circular brightness distributions and three "spots" of different sizes superposed (one brighter than the underlying photosphere and two that are cooler). `UniDisk222pc` has a uniform (circular) disk diameter of 80 mas and a flux density at 46.1 GHz of 28.0 mJy, similar to those of the RSG star Betelgeuse as measured with the VLA at 7 mm (Lim et al. 1998). `UniDisk1kpc` is an additional version appropriately scaled to a distance of 1 kpc. Both sources are located at the J2000 sky coordinates of RA=$02^{\rm h}$ $00^{\rm m}$, DEC=$-02°$ $00'$, which were intentionally chosen to result in a slightly elliptical dirty beam.

The second and third series of models we explored are based on more physically-motivated images created by 3D hydrodynamic simulations of AGB and RSG star atmospheres from Freytag et al. (2017) and Chiavassa et al. (2009). Our adaptions of these models are referred to as the `Freytag` and `Chiavassa` models, respectively, in our previous memo (Akiyama & Matthews 2019). These models are based on near-infrared images from 3D hydrodynamic simulations since no detailed, high-resolution models are currently available that predict the appearances of AGB or RSG stars at millimeter wavelengths. However, our adoption of the near-infrared models as morphological templates for the radio emission is motivated by the growing evidence based on recent VLA and ALMA imaging that radio photospheres are time-variable and non-uniform in surface brightness (e.g., O'Gorman et al. 2015; Matthews et al. 2015, 2018b; Vlemmings et al. 2019), and the origins of these behaviors may be intricately linked with those that give rise to the complex and time-varying appearance of the star at near-infrared and shorter wavelengths (e.g., Matthews et al. 2018b). While the detailed structures of radio photospheres at millimeter wavelengths are poorly constrained, the imaging simulations with these models allow challenging tests for the anticipated stochastic and complex morphology of the brightness distributions.

The `Freytag` model, simulating the time-variable images of a 1 $M_\odot$ AGB star, is based on model st28gm06n25 from Freytag et al. (2017), which has a bolometric luminosity L=6890 $L_\odot$, a mean effective temperature $T_{\rm eff}$=2727 K, and a pulsation period P=1.388 yr. The location of the star is assumed at a J2000 sky position of RA=$02^{\rm h}$ $19^{\rm m}$, DEC=$-02°$ $58'$ and a distance of ∼150 pc. We scaled the images to subtend a mean angular diameter of ∼50 mas and have an integrated flux density of 10 mJy at 46.1 GHz.

The `Chiavassa` model, simulating the time-varying appearance of a 12 $M_\odot$ RSG star, is based on the H-band model st35gm03n07 in Chiavassa et al. (2009) with a bolometric luminosity L=93,000 $L_\odot$, a mean effective temperature $T_{\rm eff}$=3490 K, and a radius R=832 $R_\odot$. We adapt this model to represent a radio photosphere whose angular diameter and flux density at 46.1 GHz

are ∼80 mas and 28 mJy, respectively, comparable to the RSG Betelgeuse, which lies at a distance of ∼222 pc (Lim et al. 1998). The star was located at a J2000 sky position also comparable to Betelgeuse (RA=05^h 55^m, DEC=+07° 24′).

2.2. *Simulations*

We performed simulated ngVLA observations of each model at 46 GHz using the `simobserve` task in `CASA` to produce model visibility data in measurement set (MS) or uvfits format. In all cases, the array configurations were taken to be the ngVLA Main Array (see Section 1) with telescope locations of the Rev C and Rev D configurations (see Section 1.2 and Figure 1).

All groundtruth model images have a pixel size of 0.04 mas, a factor of ∼25 times smaller than the angular resolution of the ngVLA Main Array at 46 GHz. To avoid edge effects, zero padding was used to create a field-of-view for each groundtruth frame of ∼0.33 arcsec per side.

In this memo, we only consider thermal noise, which was added using the prescription outlined in Carilli et al. (2017). All of our simulations assumed dual polarizations (resulting in Stokes I images) and a center observing frequency of 46.1 GHz ($\lambda \approx 7$ mm), allowing direct comparisons with both real and simulated observations from the current VLA. For noise calculation purposes, we assume a total bandwidth of 10 GHz per Stokes (half the nominal value expected for the ngVLA; see Selina et al. 2018). The synthetic observations ranged from 2–4 hours in duration and were assumed be centered on the time of the source transit.

The resulting *uv*-coverages for the `Chiavassa` model are shown in Figure 2 for both the Rev C and Rev D configurations. Figure 2 clearly shows that the Rev D configuration provides more symmetric *uv*-coverage than Rev C. The overall extension of *uv*-coverage is more uniform, which would enhance the circular symmetry of the synthesized beam pattern. Furthermore, the dense clusters of spatial frequencies created by baselines between the central core and outer intermediate/long-baseline antennas are more evenly spread in the Rev D configuration. See Section 3.2 for the resultant synthesized beams at each *uv*-weighting.

3. IMAGE RECONSTRUCTIONS

3.1. *RML Imaging*

For our RML imaging investigations, we used `SMILI`[2] (Akiyama et al. 2017a,b), a Python-interfaced open-source imaging library primarily developed for the Event Horizon Telescope (EHT) that was used in our previous memo (Akiyama & Matthews 2019). Simulated data (see Section 2) were exported to uvfits files from `CASA` and loaded into `SMILI` for imaging and analysis. Since visibility weights in uvfits files from `CASA` do not reflect actual thermal noise, they were re-evaluated using the scatter in visibilities within 1 hour blocks using the `weightcal` method. Images were then reconstructed with full complex visibilities.

The most relevant parameters for `SMILI` imaging (or for RML methods more widely) are the pixel size, the field-of-view of the image, and the choice and weights of regularization functions. We adopted a pixel size of 0.2 mas and a field-of-view of 300 pixels for all of the models. For the uniform disk models (`UniDisk222pc`, `UniDisk1kpc`) and `Chiavassa` model, we adopted Total Variation (TV) regularization at the regularization parameter of 10^3. TV regularization leads to an edge-preserved smooth image (e.g. Akiyama et al. 2017a,b), well matched with the anticipated brightness distributions for these models. For the `Freytag` model, we adopted a relative entropy term with a flat prior at a regularization parameter of 10^{-4}. This is a classical regularization function used for the Maximum Entropy Method (MEM) known to have a good performance for the edge-smoothed brightness distribution. For either of the regularization parameters, a higher value results in stronger regularization on the reconstructed image, leading to a more piece-wise smooth image.

Table 1. The parameters of the synthesized beams shown in Figure 3.

Array Config.	*uv*-weighting	θ_{maj} (mas)	θ_{min} (mas)	θ_{PA} (°)
Rev C	Uniform	2.0	1.4	7.0
	Robust	7.0	3.8	10.1
	Natural	14.0	11.1	1.8
Rev D	Uniform	1.7	1.4	-0.5
	Robust	3.5	2.3	-29.3
	Natural	12.0	11.2	3.4

3.2. *Multi-scale CLEAN*

For our `CLEAN` imaging tests, we used the `CASA` 5.8.0-109 version of `MS-CLEAN` as implemented via the "`tclean`" task. A general overview of `MS-CLEAN` can be found in e.g., Cornwell (2008) (see also Rich et al. 2008). For all `CLEAN` images presented, we adopted a loop gain of 0.1, a cell size of 0.2 mas, and 10,000 `CLEAN` iterations. No `CLEAN` boxes were used. For each model and array configuration, we tested uniform weighting,

[2] https://github.com/astrosmili/smili

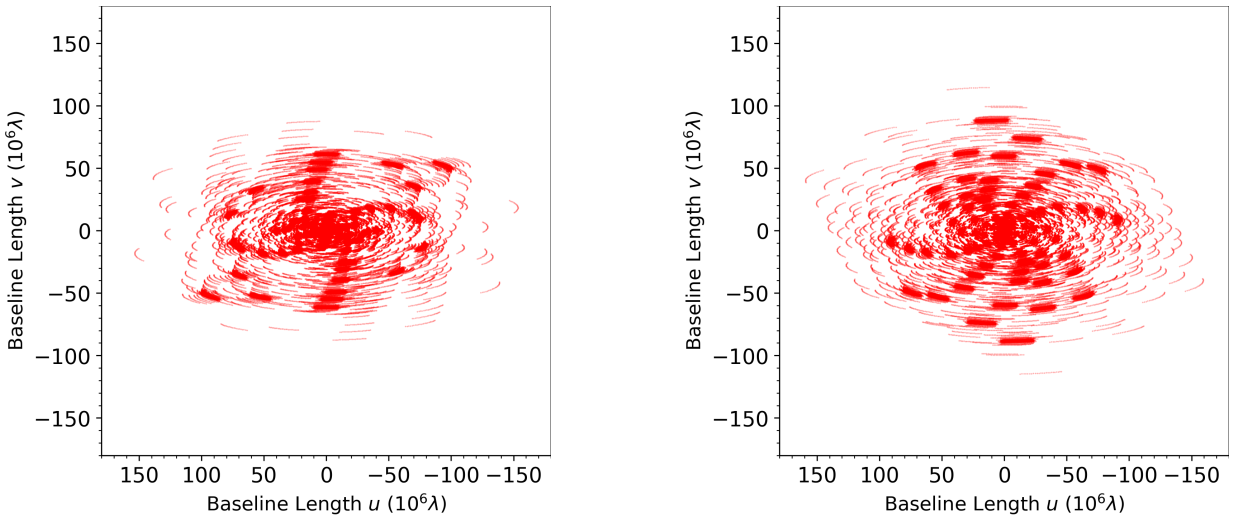

(a) Rev C Configuration

(b) Rev D Configuration

Figure 2. Example uv-coverages of the `Chiavassa` model at 46 GHz ($\lambda \approx 7$ mm). The source is located at a declination of $\sim +7^{\circ}$ (see Section 2 for details). Panels (a) and (b) show uv-coverages of the Rev C and Rev D ngVLA Main Array configurations, respectively.

natural weighting, and robust weighting with a robust parameter of zero to show the intermediate weighting between uniform and natural weightings (Briggs et al. 1999).

In Figure 3, we show the synthesized beams for the `Chiavassa` model for each weighting and array configuration, whose FWHM sizes are summarized in Table 1. In Figure 4, we show corresponding two-dimensional intensity slices across the beams. Regardless of the uv-weighting, the Rev D configuration provides a more circularly symmetric beam pattern (Figure 4), even for a low declination source, as indicated by uv-coverage (Figure 2). Furthermore, there are modest improvements in the Rev D configuration on the level of the envelope function for side lobes in all uv-weightings (Figure 4), brought by the more uniform distributions of the dense clusters of baselines in uv-space between the central core and outer antennas.

Despite the moderate improvement in Rev D's synthesized beam, the non-Gaussianity of the beam is persistent in both robust and natural weighting (Figure 3 and 4). The synthesized beams for both of these choices of uv-weighting comprise a sharp milliarcsecond-scale primary component superposed on a plateau with long tails extending over scales larger than the primary component, which are consistent with those from earlier Main Array configurations (Carilli 2017).

4. RESULTS

Figure 5 shows the groundtruth images and the `SMILI` reconstructions, which are convolved with the same Gaussian beam for the Rev D configuration in uniform weighting[3] to match the resolution across the groundtruth and reconstructions from different array configurations. Comparing the results of imaging using both Rev C and Rev D array configurations, there are not many noticeable differences for the `Freytag`, `Chiavassa` and `UniDisk222pc` models. The `UniDisk222pc` model appears slightly more uniform in shape for the rev D reconstructions when looking at the North-Western and South-Eastern edges of the star. For the `UniDisk1kpc` model, the Rev D reconstruction shows slightly better reconstruction with a more uniform brightness and better localization of a bright spot at the Eastern edge of the disk.

Figure 6 shows the `CASA` reconstructions for each stellar model with both array configurations using uniform, robust, and natural weightings. Overall, the natural weighting reconstructions lose most, if not all, of the compact stellar structure for both arrays. Although the loss in the angular resolution is expected by its definition, for both `Chiavassa` and `RSD222PC` models, where the structure is more extended than the fitted beam size, natural weighting does not allow the reconstruction of a uniform circular disk and instead artificially creates an X-shape structure. For robust weighting, the Rev D reconstructions provide clearly better reconstruc-

[3] RML methods often provide piece-wise smooth images, even without blurring the beam, which may provide high fidelity images at a modest superresolution. Please see our previous memo (Akiyama & Matthews 2019) for the unblurred groundtruth images and RML reconstructions.

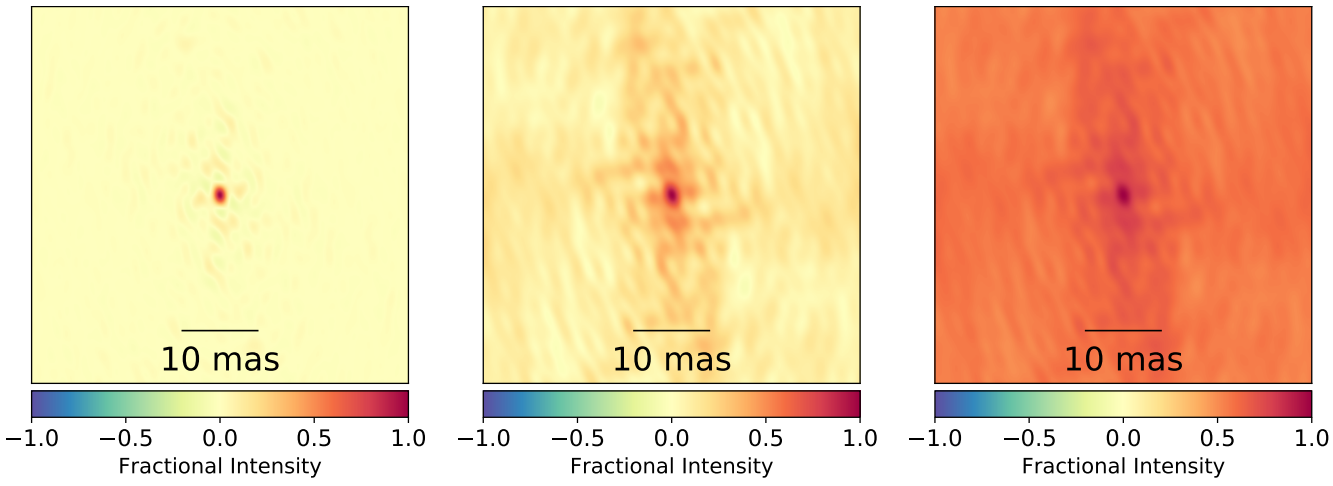

(a) Rev C Configuration, uniform weighting

(b) Rev C Configuration, robust weighting

(c) Rev C Configuration, natural weighting

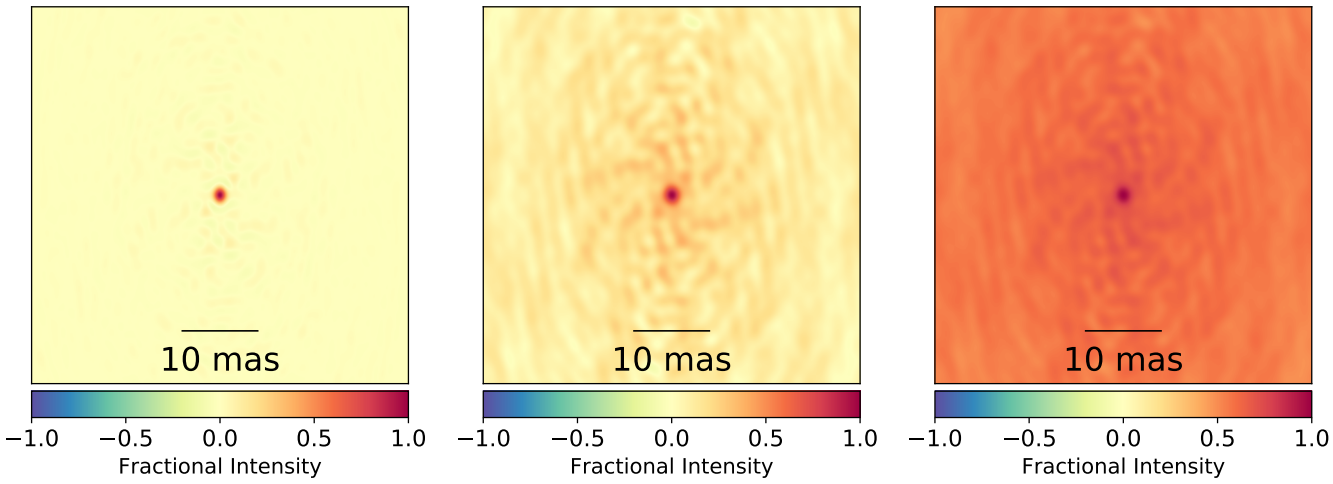

(d) Rev D Configuration, uniform weighting

(e) Rev D Configuration, robust weighting

(f) Rev D Configuration, natural weighting

Figure 3. The synthesized beams at different *uv*-weighting for both array configurations, corresponding to *uv*-coverages shown in Figure 2. The top panels (a-c) show the synthesized beams for the Rev C configuration, while the bottom panels (d-f) show those for the Rev D configuration. From the leftmost to rightmost panels, the synthesized beams for uniform, robust and natural weighting, respectively, are shown. The robust parameter for the robust weighting is set to zero to show the intermediate weighting between uniform and natural weightings. See Table 1 for FWHM sizes of each beam and Figure 4 for the linear slices of each beam along the RA and Dec axes.

tions across all four models at finer resolutions than the Rev C configuration. The uniform weighting reconstructions do not provide substantial differences for all four models.

For a more quantitative analysis with matching the resolution of images from different techniques and different array configurations, in Figure 7 we show characteristic levels of reconstruction errors at each spatial scale using the normalized root-mean-square error (NRMSE; Chael et al. 2016) for both array configurations and all reconstructions except for `MS-CLEAN` images at natural weighting. NRMSE is defined by

$$\mathrm{NRMSE}(\mathbf{I}, \mathbf{K}) = \sqrt{\frac{\sum_i |I_i - K_i|^2}{\sum_i |K_i|^2}}, \tag{1}$$

where $\mathbf{I}$ is the image to be evaluated, and $\mathbf{K}$ is the reference image. We adopt the non-convolved groundtruth image as the reference image, and evaluate NRMSEs of the groundtruth and reconstructed images convolved with an elliptical Gaussian beam equivalent to the one appropriate for uniform weighting with the Rev D configuration. The curve for the groundtruth image shows the errors caused by the limited angular resolution. As

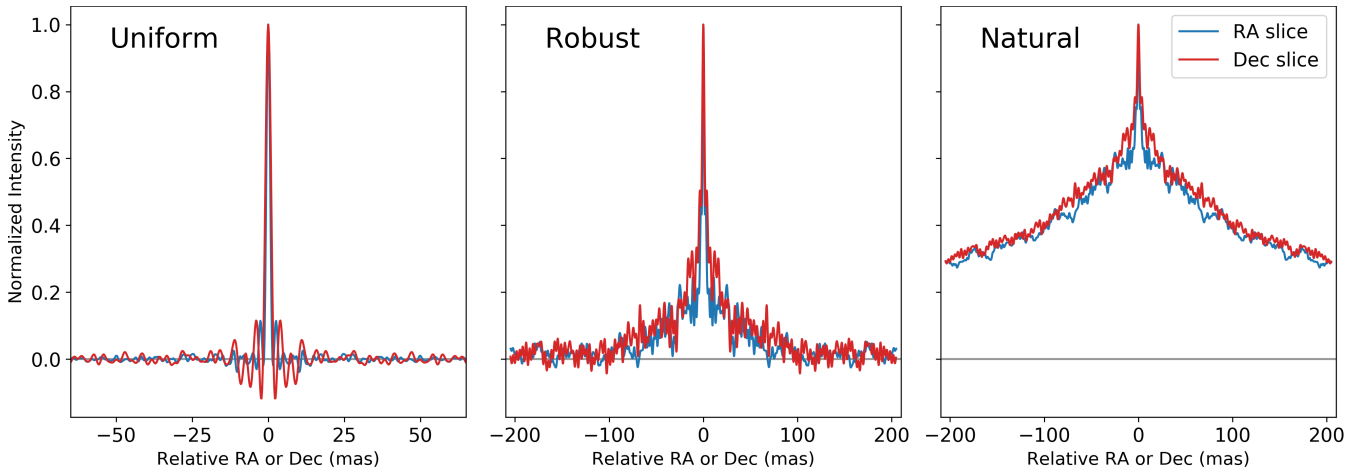

(a) Rev C Configuration

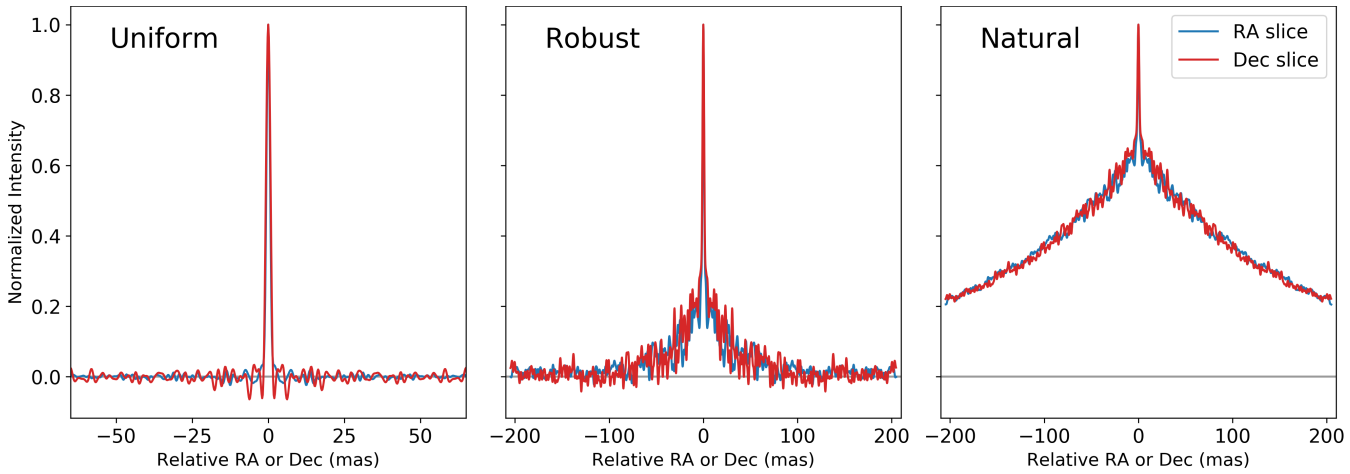

(b) Rev D Configuration

Figure 4. The linear slices of the synthesized beams shown in Figure 3, along the RA (blue line) and Dec (red line) axes. The top panel (a) shows the slices for the Rev C configuration, while the bottom panel (b) shows those for the Rev D configuration.

shown by the vertical lines, the improvement in the beam size with the Rev D configuration is more significant with the robust weighting.

Figure 7 shows that, even after matching resolutions, the Rev D configuration provides reconstructions with lower NRMSE for robust weighting, suggesting that CLEAN components are well modeled with the Rev D configuration. However, the relative improvement at the same resolution is less than that provided by the improvement in the angular resolutions, which one can see by taking differences in NRMSE values at the cross points of the vertical lines and NRMSE curves. This indicates that the Rev D's improvement in the image appearance shown in Figure 6 for robust weighting is primarily attributed to its finer beam size. For uniform weighting, the Rev C and Rev D reconstructions do not give substantial differences, even at the same resolution or even considering the slight improvement in the beam size.

RML reconstructions with `SMILI` show almost identical NRMSE curves for all models, which is consistent with the visual appearances shown in Figure 5. These demonstrate resiliency of the performance for different array configurations. Consistent with our previous work (Akiyama & Matthews 2019), RML reconstructions with `SMILI` outperform `MS-CLEAN` reconstructions with `CASA` for a wide range of spatial scales, including the nominal resolution at uniform weighting. An exception is the `Freytag` model with its many compact emission features.

5. SUMMARY

We have presented a study exploring stellar imaging with the ngVLA, continued from the study of Akiyama & Matthews (2019). In this memo, we evaluated the

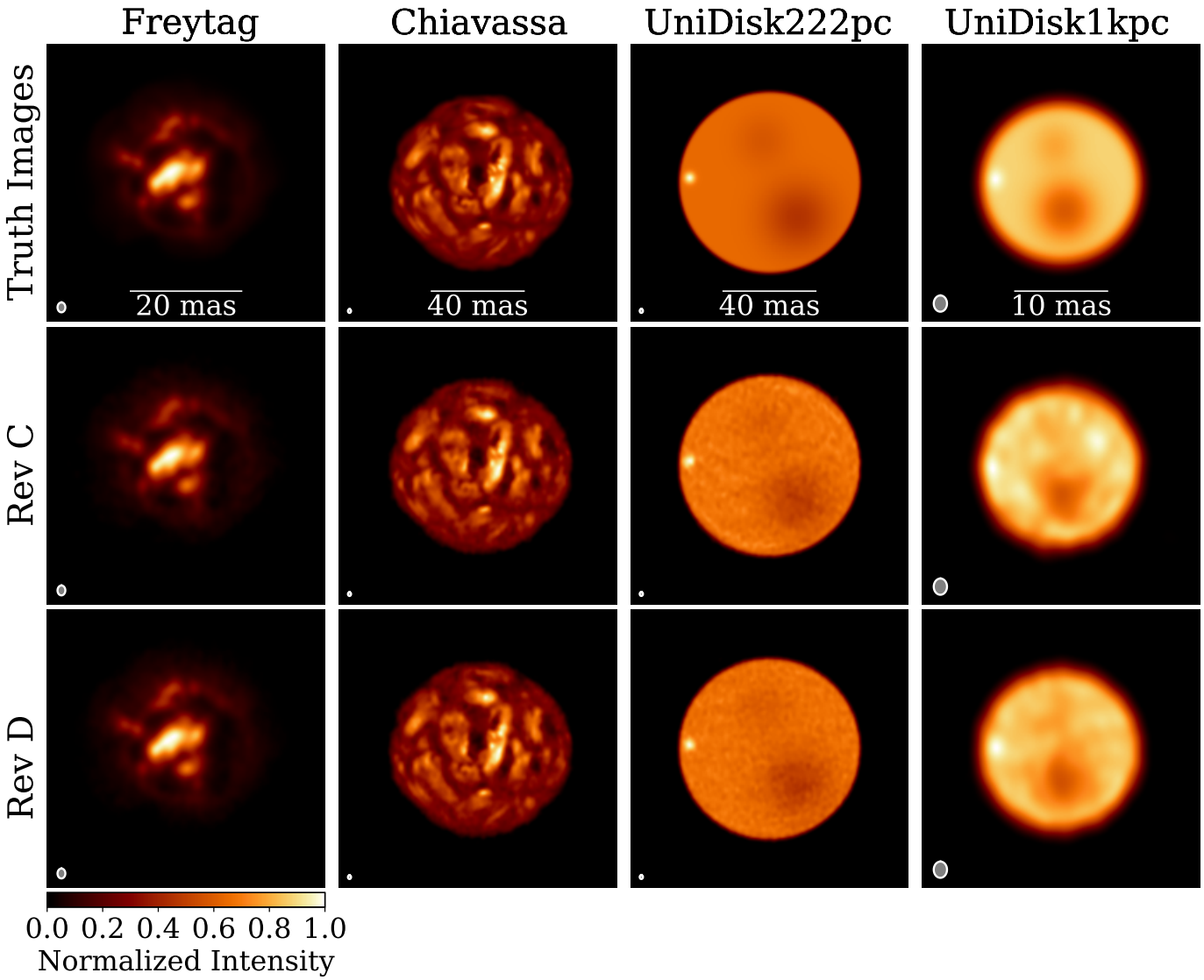

Figure 5. The groundtruth images and corresponding `SMILI` reconstructions for Rev C and Rev D configurations for four stellar models. Here, images of each model are blurred at the Gaussian beam for the Rev D configuration in uniform weighting used in `MS-CLEAN` reconstructions.

imaging performance with an updated version of the Main Array configuration (Rev D) and of `MS-CLEAN` imaging at different *uv*-weightings. Here are the main results of this work:

1. The Rev D configuration provides better *uv*-coverage, resulting in a modest improvement in the synthesized beam regardless of the choice of *uv*-weighting. The synthesized beam has a better circular symmetry and a lower tail of side lobes.

2. Both RML and uniform-weighted `MS-CLEAN` reconstructions provide high-fidelity reconstructions for all stellar models adopted in this work with both the Rev D and the previous Rev C configurations, demonstrating that the capability of stellar imaging does not significantly depend on the configurations of the Main Array.

3. For `MS-CLEAN` imaging, the Rev D configuration provides visually noticeable improvement in the recovery of the complex morphology in detailed stellar models when adopting robust weighting. The NRMSE analysis with the matched resolutions indicates that this is primarily attributed to the finer restoring beam rather than the better modeling of CLEAN components.

4. Stellar imaging with `MS-CLEAN` using natural weighting is severely limited by the highly non-Gaussian beam, and this problem remains with the Rev D configuration. The highly non-Gaussian

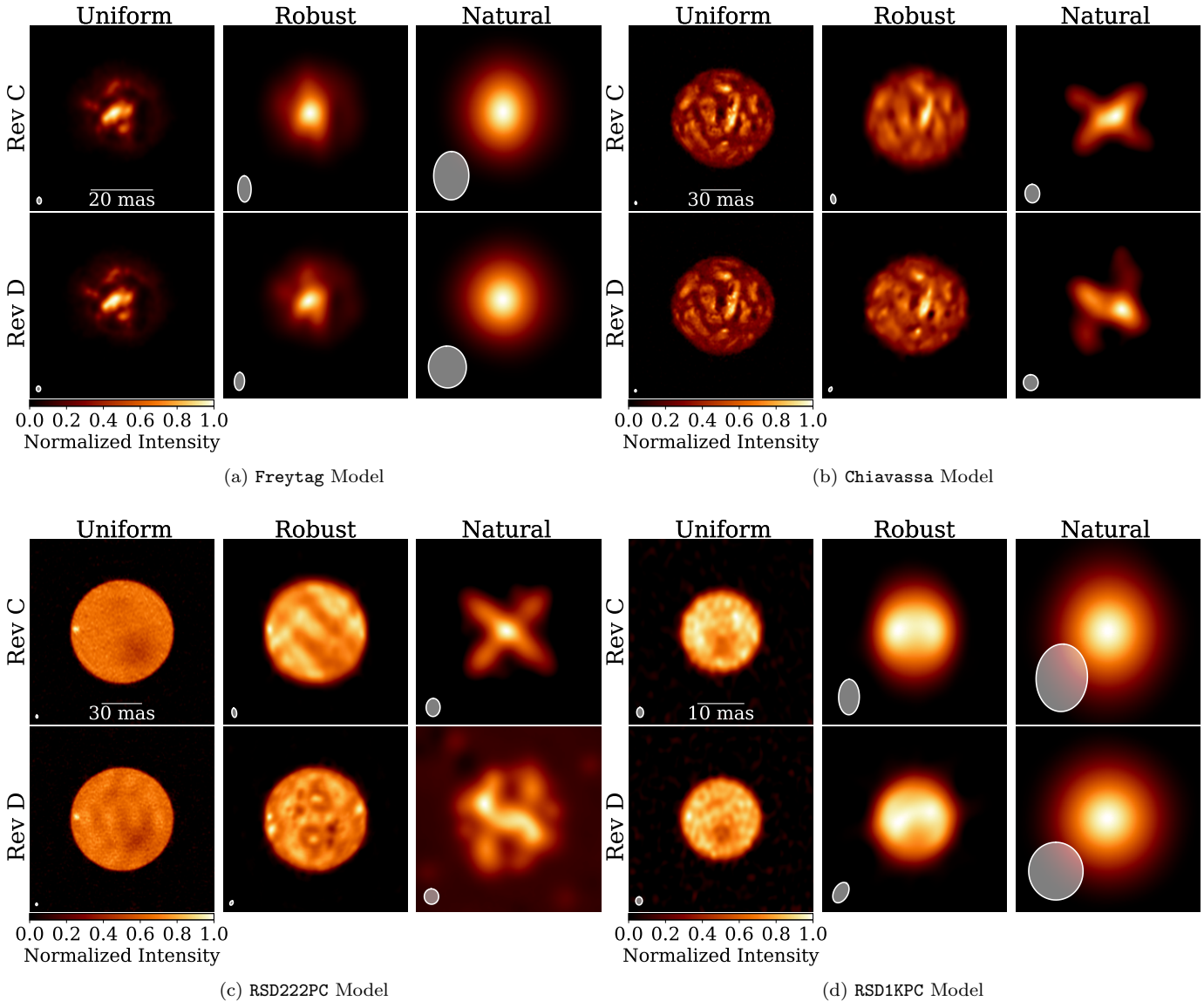

(a) `Freytag` Model

(b) `Chiavassa` Model

(c) `RSD222PC` Model

(d) `RSD1KPC` Model

Figure 6. `MS-CLEAN` reconstructions at different uv-weightings for both array configurations.

nature of the synthesized beam still persists with both robust and natural weightings in the Rev D configuration, and may induce artifacts in the `MS-CLEAN` reconstructions, even if the source structure is larger than the corresponding angular resolution. It may severely limit the capability of natural weighting for what it was traditionally considered to enhance — for instance, the fidelity of imaging more extended emission from a surrounding nebula or circumstellar material around a star, or the accurate recovery of the total flux for a given angular resolution.

5. RML images are almost identical between the Rev D and previous Rev C configurations for all four stellar models considered here, demonstrating the resiliency of its performance over different configurations. The RML methods are shown to have better or comparable performances than `MS-CLEAN` in the presented simulations, consistent with our previous work presented in Akiyama & Matthews (2019).

Our simulations imply that the Rev D configuration will provide a better imaging capability compared with previously proposed Main Array configurations, and they continue to demonstrate that RML methods are an attractive choice for imaging, even for the improved array configuration.

We note that the improvement of imaging capability provided by the Rev D configuration may be more significant for more realistic cases with residual calibration

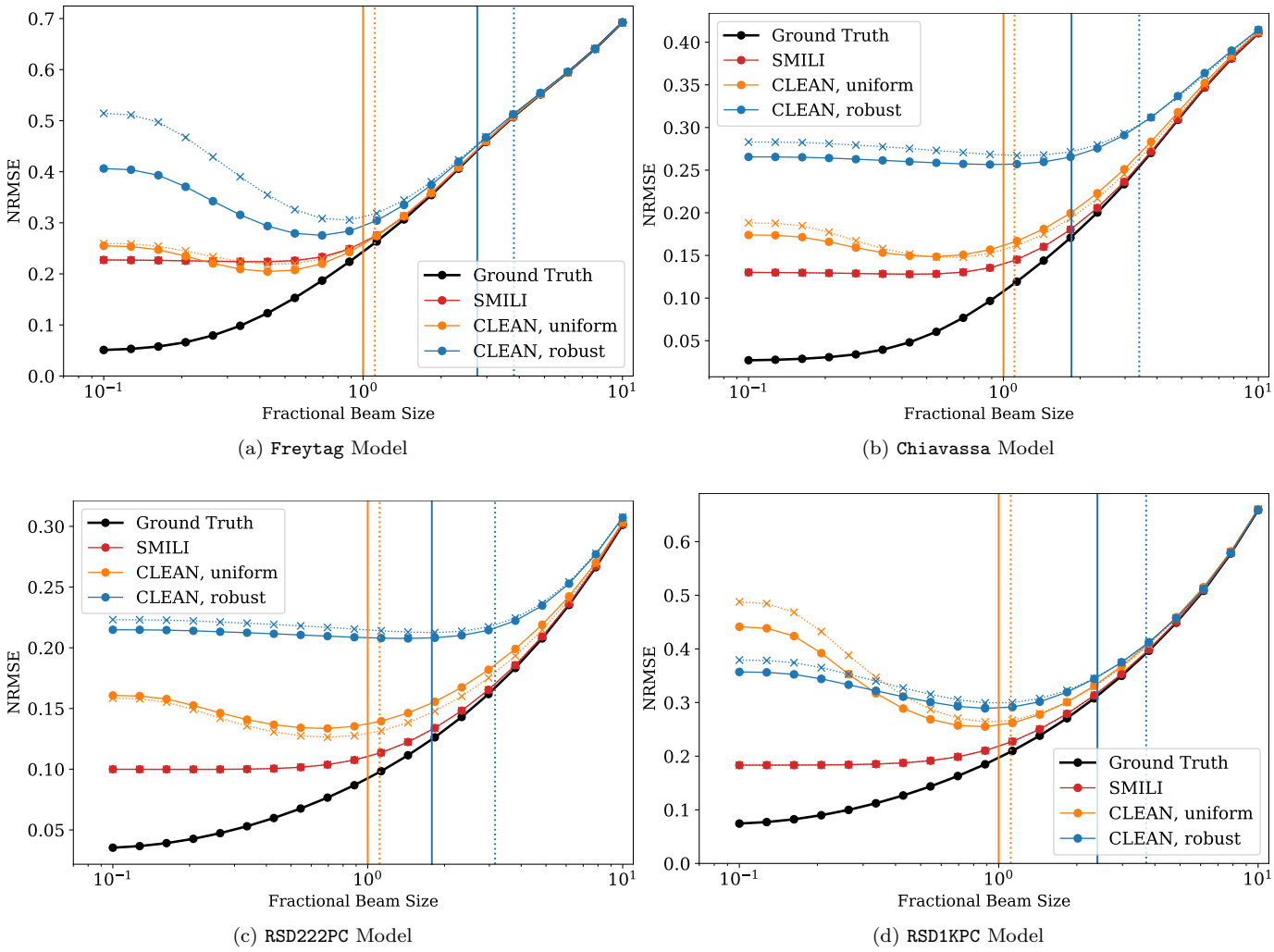

(a) `Freytag` Model

(b) `Chiavassa` Model

(c) `RSD222PC` Model

(d) `RSD1KPC` Model

Figure 7. The normalized root-mean-square errors (NRMSEs) of reconstructions as a function of the restoring beam size. Each NRMSE curve was calculated between the corresponding beam-convolved image and the *non-convolved* groundtruth image adopted as the reference. The beam size on the horizontal axis is normalized to that of uniform weighting of the Rev D configuration used in `CASA` imaging. The solid lines show the NRMSE curves for the Rev D configuration, while the dotted lines show those for the Rev C configuration. Each vertical line indicates the angular scale giving the same beam solid angle for the array configuration with the corresponding line style as the *uv*-weighting of the corresponding line color.

errors and where the better synthesized beam may be helpful in distinguishing true signals from noise while `CLEAN`ing. In future work, we will further study more realistic cases with residual calibration errors and examine spectral line imaging capabilities for the Rev D configuration as outlined in Akiyama & Matthews (2019).

ACKNOWLEDGMENTS

We thank Chris Carilli, Brian Mason and Eric Murphy for sharing the Rev D configuration, which motivates this work. This work was supported by the ngVLA Community Studies program, coordinated by the National Radio Astronomy Observatory (NRAO), which is a facility of the National Science Foundation (NSF) operated under cooperative agreement by Associated Universities, Inc. Developments of `SMILI` at MIT Haystack Observatory have been financially supported by grants from the NSF (AST-1440254; AST-1614868; AST-2034306). The Black Hole Initiative at Harvard University is financially supported by a grant from the John Templeton Foundation. Special thanks to the Barry Goldwater Scholarship and Excellence in Education Foundation.

REFERENCES

Akiyama, K., & Matthews, L. D. 2019, ngVLA Memo, No. 66, arXiv:1910.00013
Akiyama, K., Kuramochi, K., Ikeda, S., et al. 2017a, ApJ, 838, 1
Akiyama, K., Ikeda, S., Pleau, M., et al. 2017b, AJ, 153, 159
Briggs, D. S., Schwab, F. R., & Sramek, R. A. 1999, in Astronomical Society of the Pacific Conference Series, Vol. 180, Synthesis Imaging in Radio Astronomy II, ed. G. B. Taylor, C. L. Carilli, & R. A. Perley, 127
Carilli, C. L. 2017, ngVLA Memo No. 16, http://library.nrao.edu/public/memos/ngvla/NGVLA_16.pdf
—. 2018, ngVLA Memo No. 47, http://library.nrao.edu/public/memos/ngvla/NGVLA_47.pdf
Carilli, C. L., Erickson, E., Greisen, E., & the ngVLA Team. 2018, The Next Generation Very Large Array: Configuration, https://ngvla.nrao.edu/download/MediaFile/91/original
Carilli, C. L., Greisen, E., Nyland, K., & Indebetouw, R. 2017, Instructions for using CASA simulator for the ngVLA
Carilli, C. L., Mason, B., Butler, B., Rosero, V., & Murphy, E. 2021, to be released as ngVLA Memo No. 92
Chael, A. A., Johnson, M. D., Bouman, K. L., et al. 2018, ApJ, 857, 23
Chael, A. A., Johnson, M. D., Narayan, R., et al. 2016, ApJ, 829, 11
Chiavassa, A., Plez, B., Josselin, E., & Freytag, B. 2009, A&A, 506, 1351
Cornwell, T. J. 2008, IEEE Journal of Selected Topics in Signal Processing, 2, 793
EHT Collaboration. 2019, ApJL, 875, L4
Freytag, B., Liljegren, S., & Höfner, S. 2017, A&A, 600, A137
Harper, G. M. 2018, in Astronomical Society of the Pacific Conference Series, Vol. 517, Science with a Next Generation Very Large Array, ed. E. Murphy, 265
Högbom, J. A. 1974, A&AS, 15, 417
Honma, M., Akiyama, K., Uemura, M., & Ikeda, S. 2014, PASJ, 66, 95
Johnson, M. D., Bouman, K. L., Blackburn, L., et al. 2017, ApJ, 850, 172
Kuramochi, K., Akiyama, K., Ikeda, S., et al. 2018, ApJ, 858, 56
Lim, J., Carilli, C. L., White, S. M., Beasley, A. J., & Marson, R. G. 1998, Nature, 392, 575
Matthews, L. D., & Claussen, M. J. 2018, in Astronomical Society of the Pacific Conference Series, Vol. 517, Science with a Next Generation Very Large Array, ed. E. Murphy, 281
Matthews, L. D., Reid, M. J., & Menten, K. M. 2015, ApJ, 808, 36
Matthews, L. D., Reid, M. J., Menten, K. M., & Akiyama, K. 2018a, AJ, 156, 15
—. 2018b, AJ, 156, 15
Menten, K. M., Reid, M. J., Kamiński, T., & Claussen, M. J. 2012, A&A, 543, A73
Murphy, E. J., Bolatto, A., Chatterjee, S., et al. 2018, in Astronomical Society of the Pacific Conference Series, Vol. 517, Science with a Next Generation Very Large Array, ed. E. Murphy, 3
O'Gorman, E., Harper, G. M., Brown, A., et al. 2015, A&A, 580, A101
Reid, M. J., & Menten, K. M. 1997, ApJ, 476, 327
—. 2007, ApJ, 671, 2068
Rich, J. W., de Blok, W. J. G., Cornwell, T. J., et al. 2008, AJ, 136, 2897
Rosero, V. 2019, ngVLA Memo No. 55, http://library.nrao.edu/public/memos/ngvla/NGVLA_55.pdf
Selina, R. J., Murphy, E. J., McKinnon, M., et al. 2018, in Astronomical Society of the Pacific Conference Series, Vol. 517, Science with a Next Generation Very Large Array, ed. E. Murphy, 15
Vlemmings, W., Khouri, T., O'Gorman, E., et al. 2017, Nature Astronomy, 1, 848
Vlemmings, W. H. T., Khouri, T., & Olofsson, H. 2019, A&A, 626, A81
Yamaguchi, M., Akiyama, K., Tsukagoshi, T., et al. 2020, ApJ, 895, 84